Acta Mech 229, 881–900 (2018)
https://doi.org/10.1007/s00707-017-2006-1

ORIGINAL PAPER

F. G. Rammerstorfer

Buckling of elastic structures under tensile loads

This paper is dedicated to the memory of Franz Ziegler

Received: 30 March 2017 / Revised: 18 May 2017 / Published online: 29 December 2017

Abstract Typically, structures fail due to buckling if loaded by compression. However, it is important to notice that–especially in lightweight structures–there are several situations in which instabilities, such as buckling or wrinkling, can be observed under tensile loads. In the present paper, a number of problems, dealing with buckling under tensile loads, are presented. Some solutions already contained in former papers of the author are reconsidered, compared to recent results, and extended. Further new results are presented. Bifurcation buckling under tensile loading of beams, plates (with and without cut-outs), rolled metal strips, thin cell walls of metal foams, and of thin metallic films on polymer substrates is treated in this paper. It is made clear that in all cases of buckling under tensile loads eventually compressive stresses are responsible for the loss of stability. Thus, one should carefully differentiate between "buckling under tension" and "buckling under tensile loads". Nonconservative loads as well as material instabilities under tension, such as necking, are not considered in this paper.

1 Introduction

In structural mechanics, loss of stability of equilibrium is generally associated with compressive loading. However, there are several instabilities associated with global tensile loading. In F. Ziegler's famous book on "Mechanics of Solids and Fluids" [1] the bifurcation of a beam, simply supported at both ends and loaded by a rigid bar in a way that the beam is under tension, is treated as an example. This example, which was earlier studied by H. Ziegler [2], has motivated the author of this paper to choose the topic "Buckling of elastic structures under tensile loads" for this paper in memory of Professor Franz Ziegler, who was his esteemed teacher and, later on, his encouraging and inspiring colleague for many years. Further motivation for choosing this topic for this paper lies in the fact that some of the author's papers on stability problems have been either co-authored or at least influenced by F. Ziegler; see, for example, [3]. As the first Ph.D. student of Franz Ziegler, to whom this paper is devoted, the author understands the presentations in this paper (some sort of revisiting related material and extending it by new results) as devotion to Professor Franz Ziegler, who died in 2016 after a rich and fruitful life as great scientist and teacher in Mechanical Sciences.

Thinking on examples for instability under tension brings necking of a tensile specimen into mind. Similar forms of material instabilities under tensile stresses may arise in metal forming of thin plates or shells if certain "forming limits" are surpassed. For instance, the formation of periodically arranged necks (localized plastic deformations) during the conical expansion of a thin circular cylindrical shell (similar to flaring of a tube [4]) represents a bifurcation from the trivial, i.e. axisymmetric deformation process.

F. G. Rammerstorfer (✉)
Institute of Lightweight Design and Structural Biomechanics, Vienna University of Technology (TU Wien), Vienna, Austria
E-mail: ra@ilsb.tuwien.ac.at

In contrast to the mentioned material instabilities, stability loss of structures under tensile loads is not that much known. Thin rectangular sheets with a cut-out or a through-crack may locally buckle in the surrounding of the cut-out and the crack, respectively, when the sheet is stretched; see, for example, [5,6]. This is due to transverse compressive membrane forces being activated where the free edges, formed by the cut-out or crack, are predominantly oriented perpendicularly to the loading direction. Buckling under global tension is also observed, if a thin square plate is stretched diagonally between two corners [7] or a thin plate is stretched by nonuniform loads [5,8]. The rather surprising buckling or wrinkling phenomenon appearing if rectangular plates without any cut-out are stretched is treated in [8,9]. Similar situations may appear on the micro-level of closed cell foams with thin cell walls (as, for example, metal foams [10,11]) if the foam is under tension. In the cold-rolling process of thin strip metal, undesired waviness can emerge frequently although the strip is under global tension [12].

In materials sciences, some other, probably less known, but interesting examples of instabilities under global tension can be found. For instance, if a strip consisting of a thin metallic film (around 100 nm thick) on a polymeric substrate (some μm thick) is stretched, local "film buckling" accompanied by delamination and progressive uplift of the film from the substrate can be observed [13].

In addition to the demonstration of the possible appearance of instabilities under global tension, it is the aim of this paper to show how stability limits can be systematically determined. In most cases, dimensionless formulations, based on Buckingham's π-Theorem [14], could be achieved. Furthermore, the perhaps unexpected post-critical behaviours related to these stability problems, calculated by computational methods, are discussed.

In the following sections, bifurcation buckling under tensile loading of beams, plates (with and without cut-outs), rolled metal strips, thin cell walls of foams, and of some nanometres thick metallic films on polymeric substrates is treated. It is shown that in all cases of buckling under tensile loads eventually compressive stresses are responsible for the loss of stability. Hence, it is important to differentiate between "buckling under tension" and "buckling under tensile loads".

2 Buckling of beam systems under tensile load

Euler buckling of beams is the paragon for bifurcation buckling of elastic structures under compression loads. One hardly would accept it, if one affirmed that straight beams may buckle under tensile loading. Nevertheless, in Ziegler's famous book on "Mechanics of Solids and Fluids" [1] one finds in Section "Stability of Equilibrium" on pages 435–436 a brief description of the example of a straight, simply supported beam, loaded in tension by an axial force acting on the structure via a rigid rod, and the "critical tensile force" is calculated there.

2.1 Ziegler's beam

Figure 1 shows a simple beam–rod system, which probably the first time has been treated by H. Ziegler [2] under "Buckling by Tension" and has also been used by F. Ziegler [1] as an example. Since this system is associated with the name "Ziegler" (H. and F. Ziegler, respectively), in the present paper, this system shall be called "Ziegler's beam".

In [1], the critical tensile force is expressed as

$$F_{\text{crit}} = \alpha^2 EI, \tag{1}$$

where α is derived from the transcendental equation

$$\tanh(\alpha l) = \alpha e/(1 + e/l), \tag{2}$$

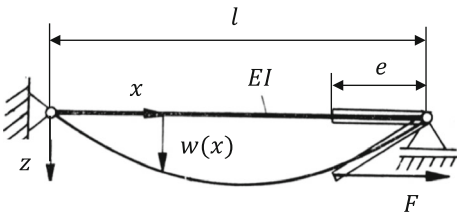

Fig. 1 Beam system under tensile loading and schematic sketch with notations as used in [1]

and EI is the bending stiffness of the beam; for e and l see Fig. 1.

Let us now consider this simple system in more detail. In order to comply with the intention of dimensionless descriptions, this "Ziegler's beam" is now reformulated using dimensionless quantities:

$$p^* = \frac{F_{\text{crit}} l^2}{EI} = \beta^2, \;\; \eta = e/l, \;\; \varphi\,(0 \text{ or } l) = \frac{\partial w}{\partial x}\,(x = 0 \text{ or } l)\;. \tag{3}$$

With these notations, the characteristic equation reads:

$$(1+\eta)\tanh\beta - \beta\eta = 0\,. \tag{4}$$

When calculating the root(s) β of Eq. (4), the dimensionless critical tensile load $p^* = \beta^2$ is determined. p^* is shown in Fig. 2 in dependence of the dimensionless quantity η .

Apparently, the beam buckles under tensile stress. However, from a different point of view one might argue that it is not the beam, which buckles, but the rigid rod of length e, which is elastically pinned at one end with a rotational spring and loaded by an axial compression force $\tilde{F}$ at the free end, loses the stability of its trivial equilibrium state. The rotational spring stiffness is contributed by the elastic beam as

$$\tilde{\gamma} = \frac{\tilde{M}\,(x = l)}{\tilde{\varphi}\,(x = l)}. \tag{5}$$

For the simple problem of bifurcation buckling of an elastically hinged rigid rod of length e, the critical force could easily be derived as $\tilde{F}_{\text{crit}} = \tilde{\gamma}/e$, and in dimensionless form

$$\tilde{p}^* = \tilde{\beta}^2 = \frac{\tilde{F}_{\text{crit}} l^2}{EI} = \frac{\tilde{\gamma} l}{\eta EI}. \tag{6}$$

If the rotational spring stiffness is calculated from the differential equation $w'' = -M/EI$ with $M\,(x)$ resulting from a torque $\tilde{M}$ acting at $x = l$, one gets $\tilde{\gamma} = 3EI/l$ and $\tilde{p}^* = 3/\eta$. The solution obtained this way is also sketched in Fig. 2, and one can see that, especially for small values of η, it hardly matches with the correct solution. One obvious reason for this discrepancy is the fact that the rotational spring stiffness $\tilde{\gamma}$ must be calculated with $M\,(x)$ depending on F according to 2nd order theory. This leads to

$$w'(x = l) = \tilde{\varphi}(l) = (\tilde{\beta}\eta\,\coth\tilde{\beta} - \eta)\tilde{\varphi}(l) \tag{7}$$

From this equation and the requirement of a nontrivial solution, i.e. $\tilde{\varphi}\,(l) \neq 0$, we come up with the eigenvalue equation for $\tilde{\beta}\,(\eta)$:

$$\tilde{\beta}\eta\,\coth\tilde{\beta} - (1+\eta) = 0. \tag{8}$$

Recasting this equation renders $(1+\eta)\tanh\tilde{\beta} - \tilde{\beta}\eta = 0$, and comparison with Eq. (4) shows that $\tilde{\beta} = \beta$. Hence, the treated buckling problem under tensile load can be interpreted as buckling of an elastically pinned rigid rod under compression loading. The l.h.s. of Eqs. (4) and (8), respectively, is antisymmetric w.r.t. $\beta = 0$ and $\tilde{\beta} = 0$, respectively, and has just one positive and one negative root, both having the same absolute value and lead, because of $p^* = \beta^2$, to the same critical load. This fact underpins the argument according to which it is the hinged rod, which–as a system with just one degree of freedom–becomes unstable under compression rather than the beam under tension. (Remark: As will be explained by considering the post-buckling behaviour later on in this subsection, a closer look shows that the virtual system of an elastically pinned rod has two degrees of freedom, a fact which has no consequence regarding the critical load; see also the Appendix.)

In order to show the fundamental difference in the buckling behaviour of this system under tensile and compression loading, respectively, let us consider the configuration according to Ziegler's beam with the exception that the external force is now acting in the opposite direction, i.e. the beam is under compression and the rod under tension. Here, the following differential equation is obtained for $\varphi\,(0) \ll 1$ from the distribution of the bending moment $M\,(x)$ according to 2nd order theory by using $w'' = -M/EI$:

$$w'' + \left(\frac{\hat{\beta}}{l}\right)^2 w = \left(\frac{\hat{\beta}}{l}\right)\varphi(0)(e - \eta x). \tag{9}$$

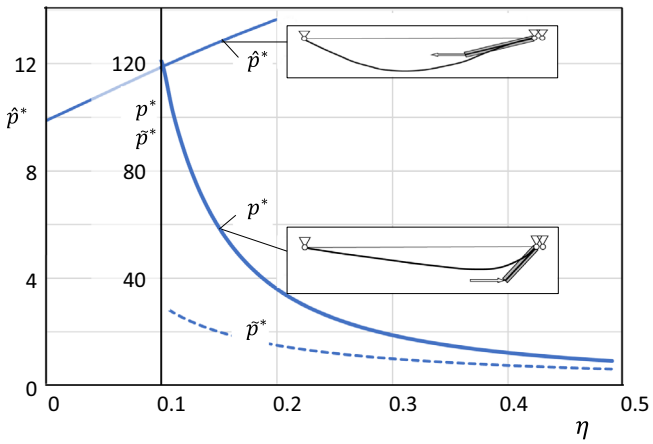

Fig. 2 Dimensionless critical tensile loads p^*, $\tilde{p}^*$, $\hat{p}^*$ as functions of $\eta = e/l$ for Ziegler's beam (see Fig. 1); inserts show bucking modes

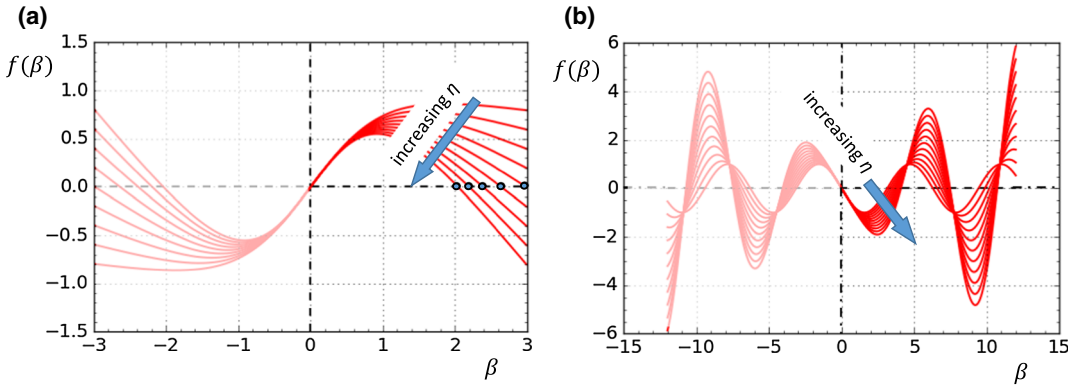

Fig. 3 Eigenvalue equations for Ziegler's beam: **a** under tensile load and **b** under compression load; curve parameters are different values of $\eta = e/l$

The general solution is

$$w = A\cos\left(\frac{\hat{\beta}}{l}x\right) + B\sin\left(\frac{\hat{\beta}}{l}x\right) + \varphi\,(0)\,(e - \eta x). \tag{10}$$

From the boundary conditions, $w(x = 0) = 0$ and $w(x = l) = 0$ follows that $A = -e\,\varphi\,(0)$ and $B = e\,\varphi\,(0)\cot\hat{\beta}$. Using these results in (10) and deriving $w'\,(x)$, one gets from the condition $w'(x = 0) = \varphi(0)$ the characteristic equation

$$(1 + \eta)\sin\hat{\beta} - \hat{\beta}\eta\cos\hat{\beta} = 0 \tag{11}$$

for a nontrivial $\varphi\,(0) \neq 0$.

In contrast to the uniqueness of the critical load of Ziegler's beam, the corresponding eigenvalue equation for the system with the external force acting such that the beam is under compression and the rod under tension has an infinite number of eigenvalues (i.e., roots of Eq. (11)), see Fig. 3b, corresponding to the infinite number of buckling modes of the beam, which here is the part of the structure which buckles. The dimensionless critical buckling load, $\hat{p}^* = \hat{\beta}^2$, is also shown in Fig. 2. By the way, here the critical load approaches the classical Euler buckling load for $\eta \to 0$.

The fundamental difference between tensile and compression loading of Ziegler's beam gets evident by considering the eigenvalue equations for both systems as shown in Fig. 3.

In order to demonstrate that this simple system exhibits a quite strange post-buckling behaviour, the results of a fully geometrically nonlinear finite element analysis are shown in Fig. 4 for the following specific choice

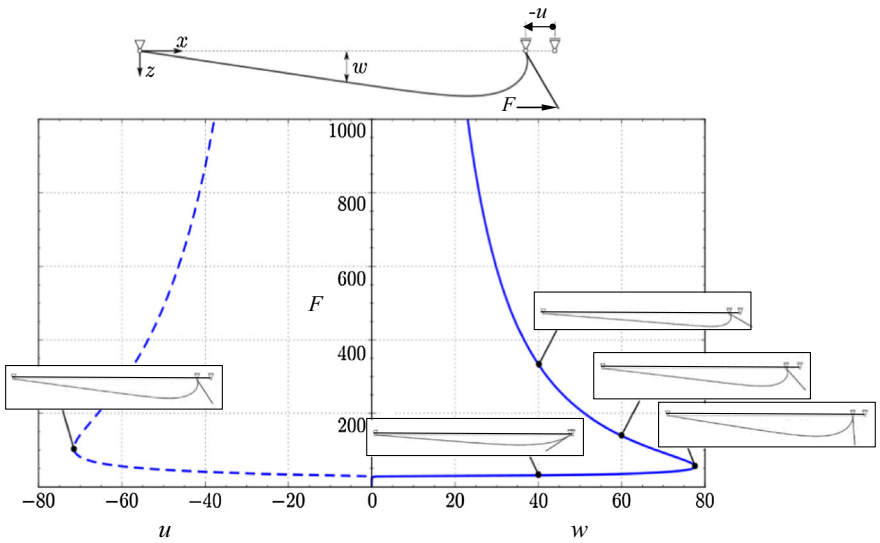

Fig. 4 Deep post-buckling behaviour of Ziegler's beam; inserts show deformed configuration; F in mm and w in N

of parameters: $l = 1.0\,\mathrm{m}$, $e = 0.15\,\mathrm{m}$, $EI = 0.5\,\mathrm{Nm}^2$. With these geometrical parameters, i.e. $\eta = 0.15$, the eigenvalue equation (4) leads to $\beta = 7.667$; hence, $p^* = \beta^2 = 58.76$, and with the given bending stiffness EI, the critical tensile load is $F_{\mathrm{crit}} = 29.4\,\mathrm{N}$.

Two facts to be gained from Fig. 4 should be emphasized:

(i) The support at that end of the beam, to which the rigid rod is attached, moves for a while oppositely to the orientation of the load, but moves back towards the initial position in the deep post-buckling range. Because of the motion of the support, the above-mentioned virtual system of an elastically pinned rod must be built with two degrees of freedom; see the Appendix.

(ii) The transverse displacement of the midspan of the beam starts increasing after surpassing the critical tensile load. However, after some further load increase the deflection diminishes more and more. One might argue that a similar behaviour can be observed for the simply supported elastica under compression load. However, one should notice that in the case of the tensile loaded beam a quite different deformation mechanism leads to the reduction in the deflection, namely some sort of smoothening down, instead of forming a loop as it happens in the case of the elastica. This smoothening effect in the post-buckling behaviour is in a sense characteristic for buckling under tensile load (see plate buckling under global tension in Sect. 3).

2.2 Some other beam–rod systems

Inspired by the closer investigation of Ziegler's beam, two more beam–rod systems under tensile loading will be considered in brief: the simply supported beam system loaded symmetrically at both ends and the cantilever beam system, both under tensile loading.

(a) Assuming a symmetric deflection of the simply supported beam system loaded symmetrically at both ends as depicted in the insert (a) in Fig. 5, the following differential equation is obtained:

$$w'' - \left(\frac{\beta}{l}\right)^2 w = -\left(\frac{\beta}{l}\right)^2 e\,\varphi(0)\,. \tag{12}$$

There, the general solution is

$$w = A\cosh\left(\frac{\beta}{l}x\right) + B\sinh\left(\frac{\beta}{l}x\right) + e\,\varphi\,(0), \tag{13}$$

from which, with the boundary conditions, $w\,(x = 0) = 0$ and $w\,(x = l) = 0$, the characteristic equation is obtained as

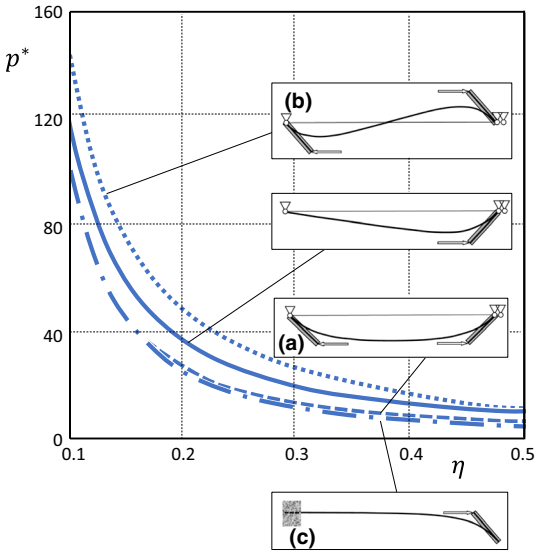

Fig. 5 Dimensionless critical tensile loads p^* as functions of $\eta = e/l$, for the systems according to the inserts in this figure, showing corresponding buckling modes

$$\sinh\beta - \eta\beta\,(\cosh\beta - 1) = 0\,. \tag{14}$$

The roots β lead, with the definitions (3), to the dimensionless critical tensile load $p^*\,(\eta)$, as it is shown in Fig. 5.

However, one has to notice that there is another deformation mode of the beam; namely, an S-shaped one (see insert (b) in Fig. 5) might be activated, too, and the above solution might be not the relevant one. Thus, let us consider this alternative system, for which the following differential equation is obtained:

$$w'' - \left(\frac{\beta}{l}\right)^2 w = \left(\frac{\beta}{l}\right)^2 (2\eta x - e)\;\varphi\,(0), \tag{15}$$

which with its general solution and the above boundary conditions leads to the characteristic equation

$$(1 + 2\eta)\sinh\beta - \eta\beta\,(\cosh\beta + 3) = 0\,. \tag{16}$$

The corresponding dimensionless critical tensile loads, depending on η, are shown in Fig. 5.

Finally, for the cantilever beam system as shown in Fig. 5 (insert c) the differential equation in analogy to Eq. (12) reads now

$$w'' - \left(\frac{\beta}{l}\right)^2 w = \left(\frac{\beta}{l}\right)^2 (e\,\varphi\,(l) - \tilde{w}) \tag{17}$$

with $\tilde{w} = w\,(x = l)$. Formulating the general solution and fulfilment of the boundary conditions, $w\,(x = 0) = 0,\ w'(x = 0) = 0$ with $w'(x = l) = \varphi(l)$ the following characteristic equation is achieved:

$$\eta\beta\sinh\beta - \cosh\beta = 0. \tag{18}$$

Figure 5 shows p^* for the cantilever beam system, too.

3 Buckling of rectangular plates under uniaxial in-plane tensile loading

In contrast to beams, which never buckle when an external axial tensile load is directly applied to the end of the beam axis, buckling of plates under external in-plane tensile edge loading is possible.

There is some literature on local buckling in the area around cut-outs of stretched plates or strips; see [5,15]. Some papers are dealing with local buckling in the area of cracks in plates under tension [6,16]. A systematic treatment of these phenomena, especially in terms of dimensionless quantities (based on Buckingham's π-Theorem [14]), is provided in Sect. 3.2 together with the consideration of the post-buckling behaviour.

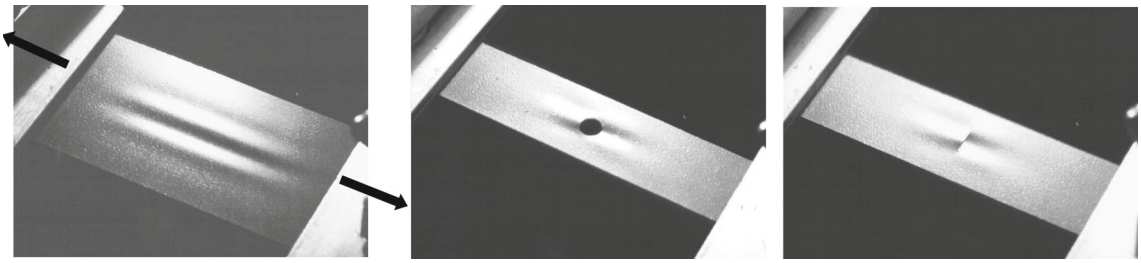

Fig. 6 Experimentally observed buckling patterns of stretched plates with and without cut-outs

It is less known that stretched plates without any cut-out or crack may buckle. This kind of buckling under tensile loading was treated in [9], and several papers followed afterwards; see, for example, the nice analytical treatment in [17]. In [18] and [19], where the decrease of the heights of the buckles in the post-buckling regime are treated, too, a number of references to recent papers on stretch buckling of rectangular plates can be found. This tensile buckling problem is shortly recalled here for the sake of completeness.

Figure 6 shows the mentioned tensile buckling phenomena in experimental considerations. There the post-buckling deformations of the plates with a hole and with a crack, respectively, correspond to the second mode shape. Obviously, this is due to predominantly antisymmetric imperfections, caused by the preparation of the specimens.

3.1 Stretched plates without cut-outs or cracks

In this Subsection, buckling of stretched plates without any cut-outs or cracks is presented, based on results achieved in [9]. Figure 7 shows the notations used as well as the distribution of the in-plane stresses σ_{yy}. One can see the appearance of areas of tensile stresses close to each of the short edges, which results from the Poisson effect, caused by hindering the movement in y-direction, and an area of compressive stresses in between, appearing due to the requirement of equilibrium (consider, for example, a cut along the symmetry axis in x-direction). For larger aspect ratios (long strips), the area of compressive stresses breaks down forming two areas of significant compressive stresses near the tensile stress areas. The distribution of the buckling waves in the post-buckling domain reflects this character of the compressive stress distribution; see the inserts in Fig. 8.

It becomes obvious again that bucking under tensile loading is due to compressive stresses.

In [9], from some analytical considerations and from parametric computational studies the dependence of the dimensionless buckling stress

$$p^* = \frac{\sigma_{\text{crit}}}{E\,(t/B)^2}; \quad p^* = p^*\,(\xi) \;\; \text{with} \;\; \xi = \frac{L}{B}, \tag{19}$$

has been found as a function of ξ for a fixed value of the Poisson's ratio, $\nu = 0.33$, which is typical for most of the metals used in lightweight design. In Eq. (19), σ_{crit} is the global tensile stress acting at the short edges as loading at the instant of buckling, t is the plate thickness and E is the Young's modulus.

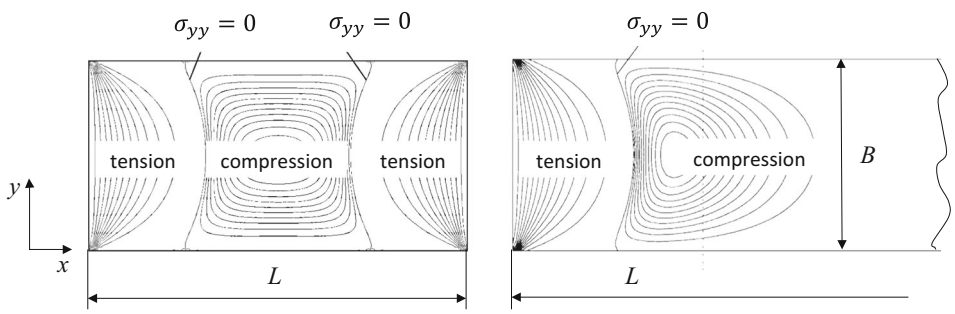

Fig. 7 Geometric notations of the stretched rectangular plate, clamped at both short edges, and the distribution of the in-plane stresses σ_{yy}; see also [9]

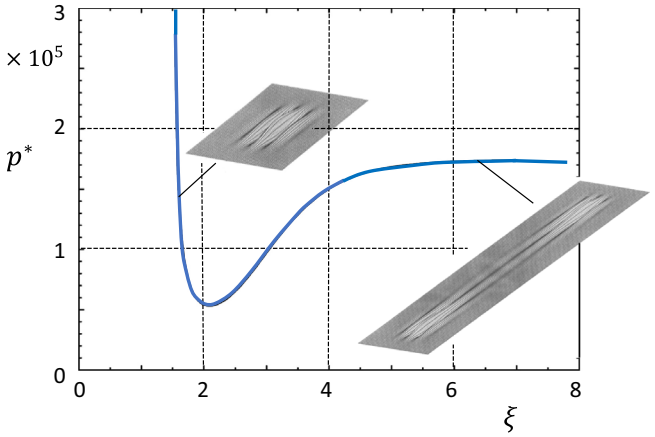

Fig. 8 Dimensionless critical tensile load as function of the aspect ratio of the plate; inserts show typical buckling patterns for short and long strips; compare [9]

By the way, p^* represents the buckling factor k in the formulation

$$\sigma_{\text{crit}} = k E \, (t/B)^2 \,, \tag{20}$$

as typically used in the engineering plate buckling literature; see, for example [20].

Buckling phenomena as described here can be also observed on the micro-level of lightweight closed cell foams under tensile load, leading to a macroscopic, i.e. homogenized stress strain behaviour appearing as if plastic deformations would take place; see Fig. 9.

3.2 Stretched plates with circular cut-outs or cracks

For configurations as shown in Fig. 10 one hardly can obtain analytical estimates for critical tensile loads at the short edges of the plate. There computational methods have been applied [21] for calculating both the stress field and the critical load intensities. However, based on the π-theorem dimensionless quantities can be found

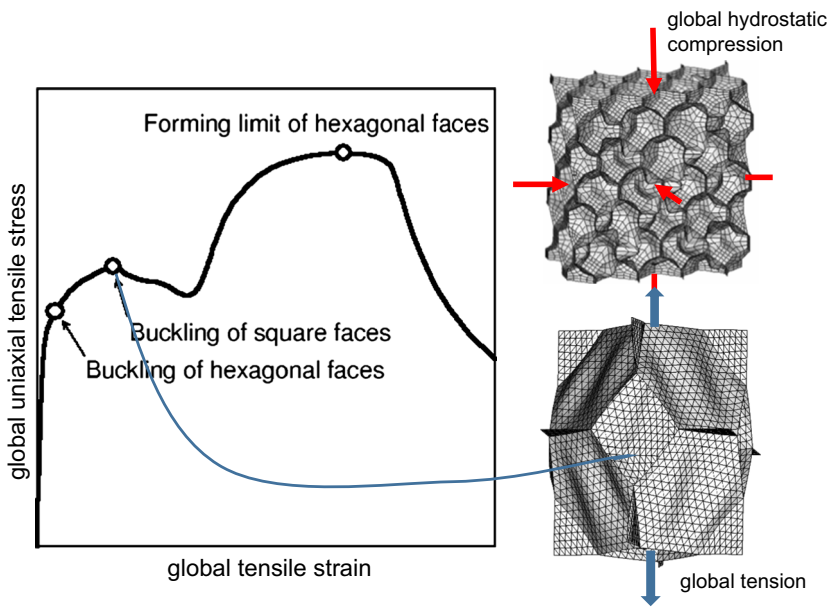

Fig. 9 Macroscopic tensile stress-strain diagram for a closed cell metal foam; microbuckling as possible reason for pseudoplastic behaviour. Cell buckling under hydrostatic pressure is shown, too; compare [10,11]

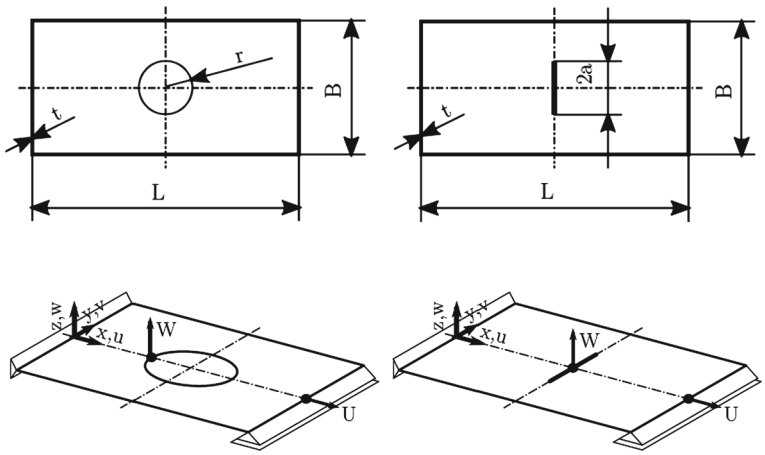

Fig. 10 Geometric notations of stretched plates with a circular cut-out or a crack

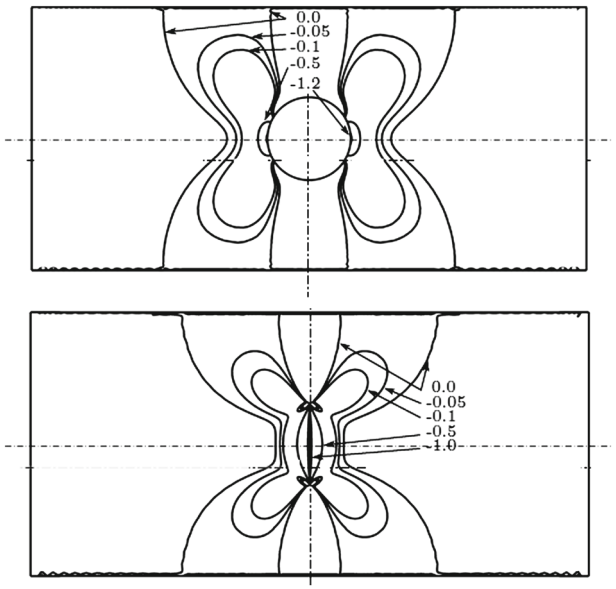

Fig. 11 Distribution of the in-plane stresses σ_{yy} and numbers represent dimensionless stress levels, normalized by the tensile stress load σ at the short edges of the plate

which allow results of parametric finite element studies to be used in a general way, as long as linear elasticity can be assumed.

The following dimensionless quantities are used in addition to those already defined in Eq. (19):

$$\rho = \frac{r}{B}; \quad \vartheta = \frac{a}{B}. \tag{21}$$

Figure 11 shows, for a given set of geometric parameters, areas of compressive stresses σ_{yy}, which eventually are responsible for local buckling under global tensile loading.

For obtaining the critical tensile load, the following eigenvalue problem

$$(\boldsymbol{K}_0 + \lambda_i \boldsymbol{K}_\Delta)\boldsymbol{\phi}_i = \boldsymbol{0}, \tag{22}$$

has to be solved. The eigenvalue λ_i corresponds to the ith buckling mode, represented by the eigenvector $\boldsymbol{\phi}_i$. Here, $\boldsymbol{K}_0$ is the tangent stiffness matrix at a load intensity σ_0, chosen to be close enough to the critical intensity σ_i^* in order to avoid the calculation of negative eigenvalues as absolute smallest ones, which would correspond to critical compression loadings. $\boldsymbol{K}_\Delta$ is the change in the tangent stiffness matrix due to a chosen

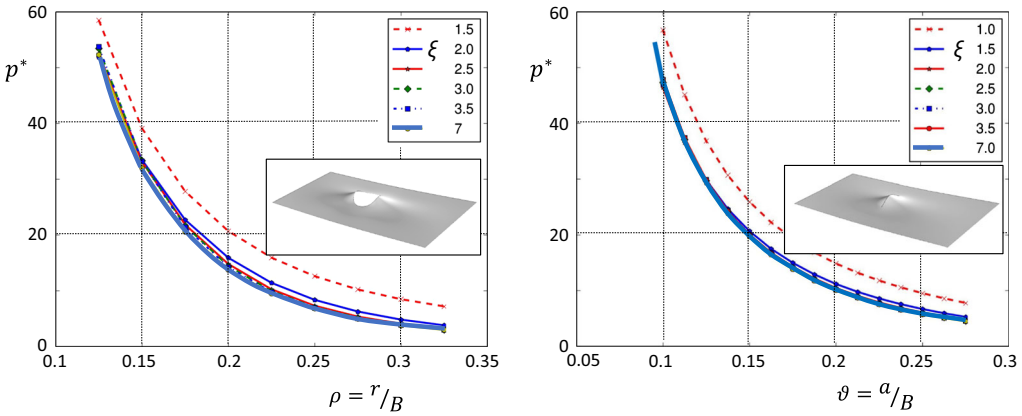

Fig. 12 Dimensionless critical tensile loads p^* in dependence of the geometrical parameters

load increment $\Delta\sigma$. Hence, the smallest critical load intensity $\sigma_1^* = \sigma_{\text{crit}} = \sigma_0 + \lambda_1 \Delta\sigma$ is relevant for buckling. This formulation has been chosen in order to avoid calculation of eigenvalues corresponding to buckling under compression loading as resulting from formulations of eigenvalue problems common in linear buckling analyses under compression loading,

$$(\boldsymbol{K}_{\text{L}} + \hat{\lambda}_i \boldsymbol{K}_{\text{g}})\hat{\boldsymbol{\phi}}_i = \boldsymbol{0}, \tag{23}$$

with $\boldsymbol{K}_{\text{L}}$ being the linear initial stiffness matrix and $\boldsymbol{K}_{\text{g}}$ the linearized geometrical stiffness matrix at reference load.

In Fig. 12, the dimensionless critical loads p^*, together with the corresponding buckling modes, are shown in dependence of ρ and ϑ, respectively, with the plate's aspect ratio ξ as parameter. As one can see, for $\xi > 3.0$ the influence of the aspect ratio L/B diminishes, and again we come up with typical buckling factor diagrams, where, in contrast to usual buckling of plates, the dimensionless geometric parameters of the cut-out and the crack, respectively, are values at the abscissa.

Studying the deep post-buckling behaviour by fully geometrical nonlinear analyses [21] reveals the interesting effect that at a certain load intensity the amplitudes of the buckles start decreasing, an observation already made in Sect. 2 for Ziegler's beam and mentioned in Sect. 3.1.

While this behaviour is shown in [18] and [19] for rectangular plates without any cut-out or crack, in the following this has now been investigated here for a plate with a circular cut-out, see Fig. 13a, and for a plate with a crack, see Fig. 13b. The plates considered here have a width of $B = 190.5$ mm. The other geometrical parameters are for the plate with cut-out: $L/B = 3.0, t/B = 0.0063, r/B = 0.157$ and for the plate with crack: $L/B = 2.5, t/B = 0.0052, a/B = 0.157$.

Similar to the observation described for Ziegler's beam in Sect. 2 of this paper, immediately after bifurcation from the trivial equilibrium path, the amplitudes of waves in the post-buckling deformations grow rapidly with slowly increasing tensile load. This first process is followed by a reduced growth rate of the buckles, and finally, the waves start to flatten out. One should, however, note that the results presented in Fig. 13 are based on the assumption of linear elastic material behaviour. Thus, they are rather of demonstrative value, because plastic or viscous effects would come into play and, at least, for the plate with a crack fracture might happen before reaching sufficiently large load intensities for observing the flattening.

4 Buckling of thin strips with residual stresses and global tension

In Sect. 3, strips, free of initial stresses, under global tensile loading are considered. In the present section, the objects of consideration are thin (infinitely long) strips with stress states resulting from residual stresses and global tension. The treatment of such situations is of great importance for a proper control of strip rolling and levelling processes. Figure 14 demonstrates schematically that deviations from a parallel rolling gap (in reality, just a few hundredth of a millimetres are sufficient to produce problems) may lead to residual stresses, large enough in order to lead to waviness of the strip if the global strip tension is reduced to a critical value. Since here it is not the increase in tensile loading, but its decrease the reason for buckling, this kind of "instability

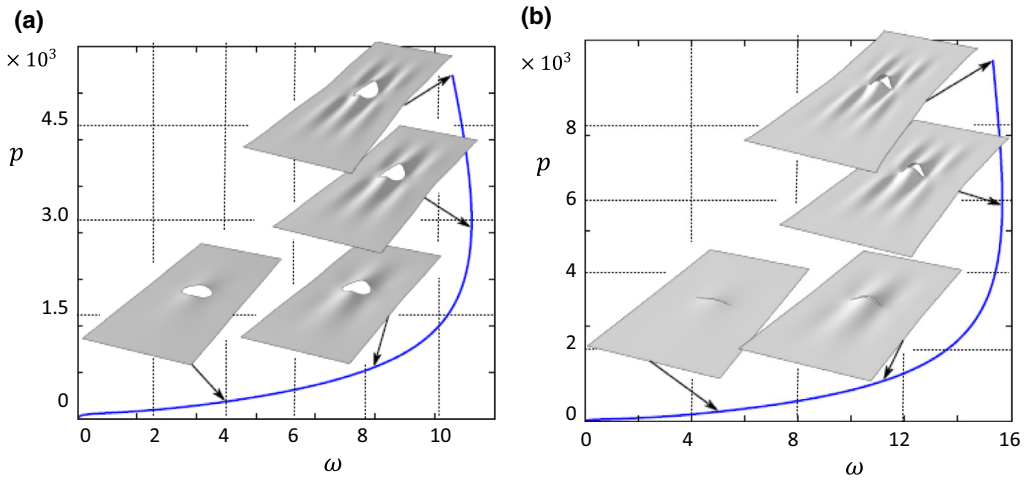

Fig. 13 Development of the amplitude of the buckles—specified example of a plate with circular cut-out and of a plate with a crack; $p := \sigma / \left[E\,(t/B)^2 \right]$, $\omega := W/t$

under global tension" is not really in the same line as the other stability problems discussed in this paper. Nevertheless, not only in papers by the author, see, for example, [12], but also in papers which have followed, as, for example, [22] and citations therein, such phenomena are mentioned in relation to "buckling under tension". This is the reason for including this small section in this paper.

In [12,24], the critical values of the global tension, at which for different intensities of the residual stresses and shapes of their distribution buckling appears, are calculated analytically. The notations are shown in Fig. 15.

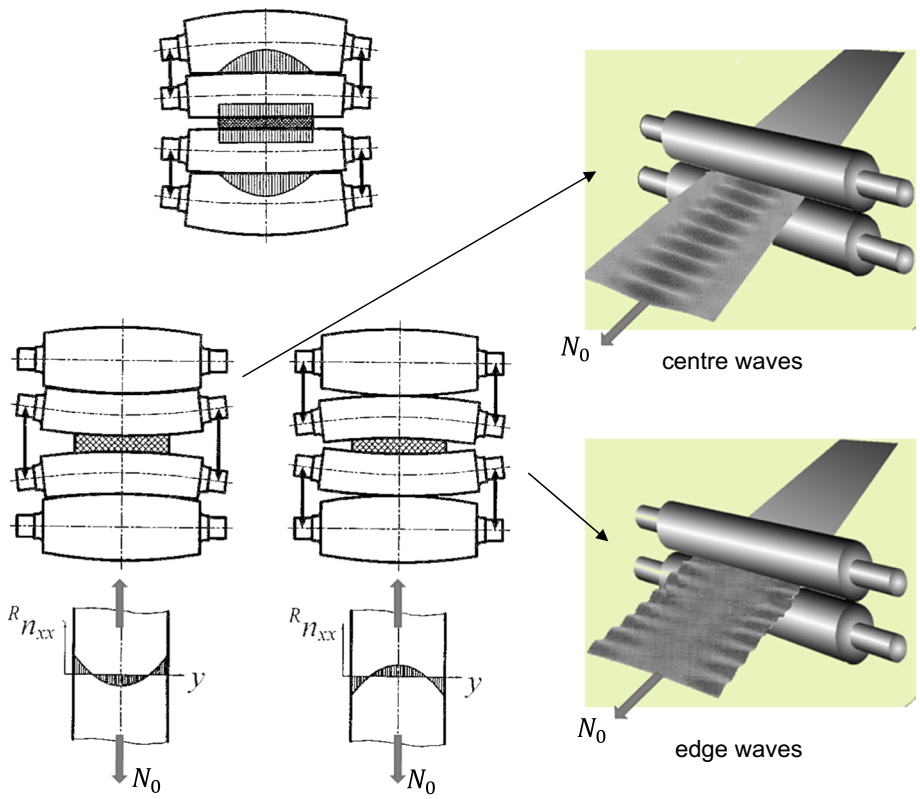

Fig. 14 Schematic demonstration of the evolution of residual stresses during rolling, leading to wavy strips during release of the global strip tension

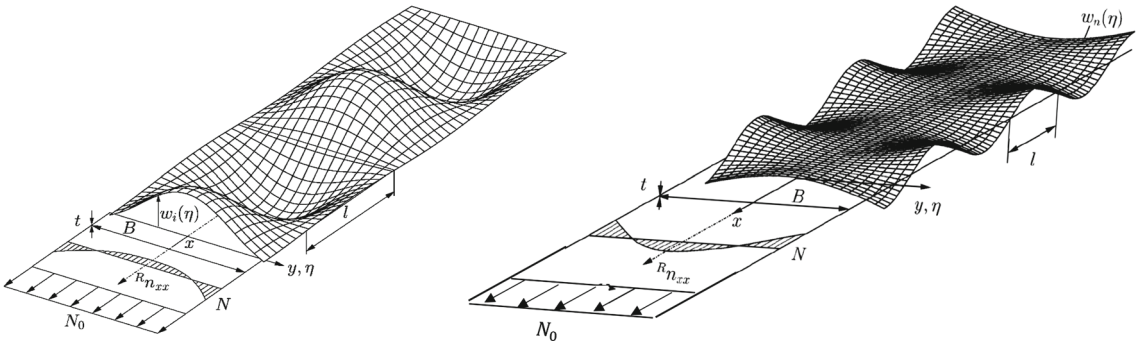

Fig. 15 Notations used in the analytical models

The strip has a bending stiffness $K = \frac{E\,t^3}{12(1-\nu^2)}$ (with E being Young's modulus, ν Poisson's ratio, t the thickness), which is loaded by a self-equilibrating residual membrane force distribution $^{R}n_{xx}(y) = N\hat{g}(y)$ and a constant global tensile force N_0 (all being forces per unit length); see Fig. 15. Hence, the membrane force distribution is given by

$$n_{xx}(y) = N\hat{g}(y) + N_0. \tag{24}$$

With

$$\eta = y/B, \quad -B/2 \le y \le B/2, \quad -1/2 \le \eta \le 1/2, \tag{25}$$

one gets

$$\hat{g}(y) \to g(\eta), \quad n_{xx} \to n_{xx}(\eta) = N\,g(\eta) + N_0. \tag{26}$$

The distribution shapes $g(\eta)$ of the residual membrane forces are described in [12,23] as follows:

For situations prone to centre wave buckling, cosine-type distributions are described as:

$$g^c(\eta) = 1 - C_m \cos^m(\pi\eta) \qquad \text{with } m = 1,\, 2, \ldots \text{ and } -1/2 \le \eta \le 1/2, \tag{27}$$

with

$$C_m = \frac{1}{2}\left[\int_0^{1/2} \cos^m(\pi\eta)\mathrm{d}\eta\right]^{-1}, \tag{28}$$

in order to ensure that the residual stresses $^{R}n_{xx}(\eta)$ are self-equilibrated.

Polynomial-type distributions, fulfilling the equilibrium requirements, are given by:

$$g^p(\eta) = \frac{1}{m}\left[(m+1)(2\,|\eta|)^m - 1\right] \quad \text{with } m = 1, 2, \ldots \tag{29}$$

Both distributions, i.e. the cosine and the polynomial one, lead to $g(\eta = \pm 1/2) = 1$. Hence, N can be defined as intensity of the residual membrane force distribution.

If buckling in terms of edge wave buckling is the problem, the typical residual membrane stress distributions can be described in the same way as for centre wave buckling problems if multiplied by -1.

In the applied Ritz–Galerkin approach, the Ritz-ansatz with just a single degree of freedom, q, for the nontrivial displacement field is, depending on whether centre or edge wave buckling is considered, again described by several parameters.

For centre wave buckling,

$$w\,(x,\eta) = q\,w_a\,(x,\eta)\,, \quad w_a\,(x,\eta) = \cos\,(a\pi\eta)\,\cos\left(\frac{\pi x}{l}\right) \tag{30}$$

or

$$w\,(x,\eta) = q\;w_n\,(x,\eta)\,, \quad w_n\,(x,\eta) = \left(1 - 12\eta^2 + 16\eta^3\right)^n \cos\left(\frac{\pi x}{l}\right), \tag{31}$$

and for edge wave buckling

$$w\,(x,\eta) = q\;w_n\,(x,\eta)\,, \quad w_n\,(x,\eta) = (2\,|\eta\,|)^n \cos\left(\frac{\pi x}{l}\right)(\mathrm{sign}\,\eta)^k$$

with $k = 1$ for the antisymmetric buckling mode and $k = 2$ for the symmetric buckling mode.

The parameters c, p, m and a, n, k as well as the still unknown half wavelength l allow a quite large variability of the shape of the residual stress distribution and of the buckling mode shapes, respectively.

The following further dimensionless quantities have been introduced:

$$\tilde{N} = \frac{N B^2}{K\pi^2}, \quad \tilde{N}_0 = \frac{N_0 B^2}{K\pi^2}. \tag{32}$$

The critical intensity of the residual stress field with a given distribution shape $g(\eta)$ is determined by c, p, m, and a given global tensile load is obtained by deriving the strain energy in the system

$$U = U_B + U_M + U_{N_0} \tag{33}$$

with

$$U_B = \frac{K}{2} \int_\Omega \left\{ \left(\frac{\partial^2 w}{\partial x^2} + \frac{\partial^2 w}{\partial y^2} \right)^2 - 2\,(1-\nu) \left[\frac{\partial^2 w}{\partial x^2} \frac{\partial^2 w}{\partial y^2} - \left(\frac{\partial^2 w}{\partial x \partial y} \right)^2 \right] \right\} \mathrm{d}\Omega, \tag{34}$$

$$U_M = \frac{1}{2} \int_\Omega \left({}^R n_{xx} + N_0 \right) \left(\frac{\partial w}{\partial x} \right)^2 \mathrm{d}\Omega\,, \tag{35}$$

$$U_{N_0} = -\frac{N_0^2 L B}{2Et}, \tag{36}$$

and looking for its stationary value by

$$\frac{\partial U}{\partial q} = 0. \tag{37}$$

This leads the strip tension for first appearance of a nontrivial solution. However, this critical global strip tension is yet a function of the still unknown wavelength as well as the other parameters describing the Ritz-ansatz for the buckling mode. Determining the minimum w.r.t. these parameters leads to the critical intensity of the residual stresses $\tilde{N}(\tilde{N}_0)$ and, vice versa, to the critical strip tension $\tilde{N}_0(\tilde{N})$, for a given intensity of the residual stresses.

Again, the formulae and diagrams have been derived in dimensionless form in order to allow a quite general use of the achieved results.

From Fig. 16, as derived in [23], the critical value of the global strip tension can be deduced for given residual stresses (determined by the shape of their distribution and their intensity). This means that from these diagrams one immediately can find to which level the global tension has to be reduced in order to cause instability of the plane configuration of the strip and development of waviness with further release of the strip tension. Furthermore, the buckling mode shape as well as the wavelength can be deduced. Let us denote this procedure, which is described in detail in [12,24], as "forward problem".

However, of much more practical importance is the "backward problem", i.e. achieving knowledge of the intensity and shape of distribution of the residual stresses in the rolled strip from observing (measuring) the critical global strip tension as well as the buckling mode shape and wavelength. In addition to, but based on solutions presented in the above-mentioned papers, a procedure is demonstrated now for solving this "inverse problem" applicable to controlling the rolling and levelling process in a way, which leads to reduced residual stresses and, hence, to improved quality of the rolled strip. Figure 17 demonstrates schematically the process of solving the backward problem:

The global strip tension is released to the critical value, i.e. to the instant, at which the first time buckles are observed (measured). This can be done even during the strip rolling process in the plant by a roller system with appropriately controlled rolling speeds. This critical global strip tension value, transformed into the dimensionless form, together with measured wavelength (again expressed in dimensionless form) and the observed (measured) shape of the buckles, i.e. either centre or edge waves, is sufficient for estimating the intensity and the distribution shape of the residual stresses in the strip.

Now, for the sake of completeness, as done so far in the previous sections of this paper, the post-buckling behaviour, i.e. the process of strip tension release and the increase in the wave amplitude, shall be demonstrated here as some further new interesting result. For this purpose, in Fig. 16 a tensile load path is added as a horizontal line at a chosen level of intensity of the residual stresses $\tilde{N}$, starting from a global tensile load $\tilde{N}_0$, which is large

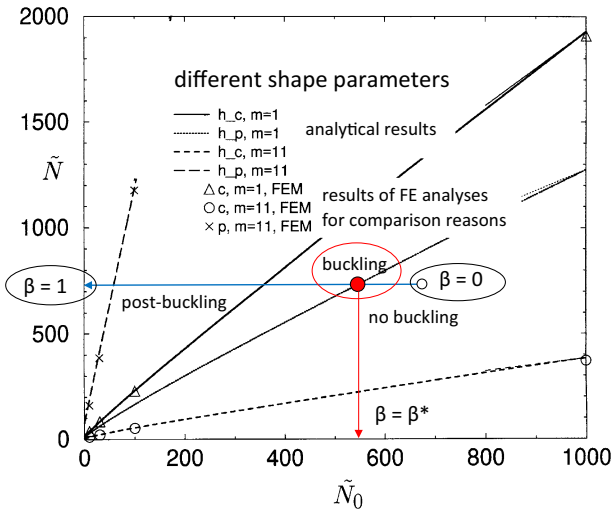

Fig. 16 Diagram showing curves representing critical combinations of residual stress intensities $\tilde{N}$ and global strip tension $\tilde{N}_0$ for different shapes of the distribution of the residual stresses along the width of the strip, characterized by specific values of the shape parameters of the residual stress distribution–shown for centre waves as example (compare [23]). The line from $\beta = 0$ to $\beta = 1$ is used in Fig. 18

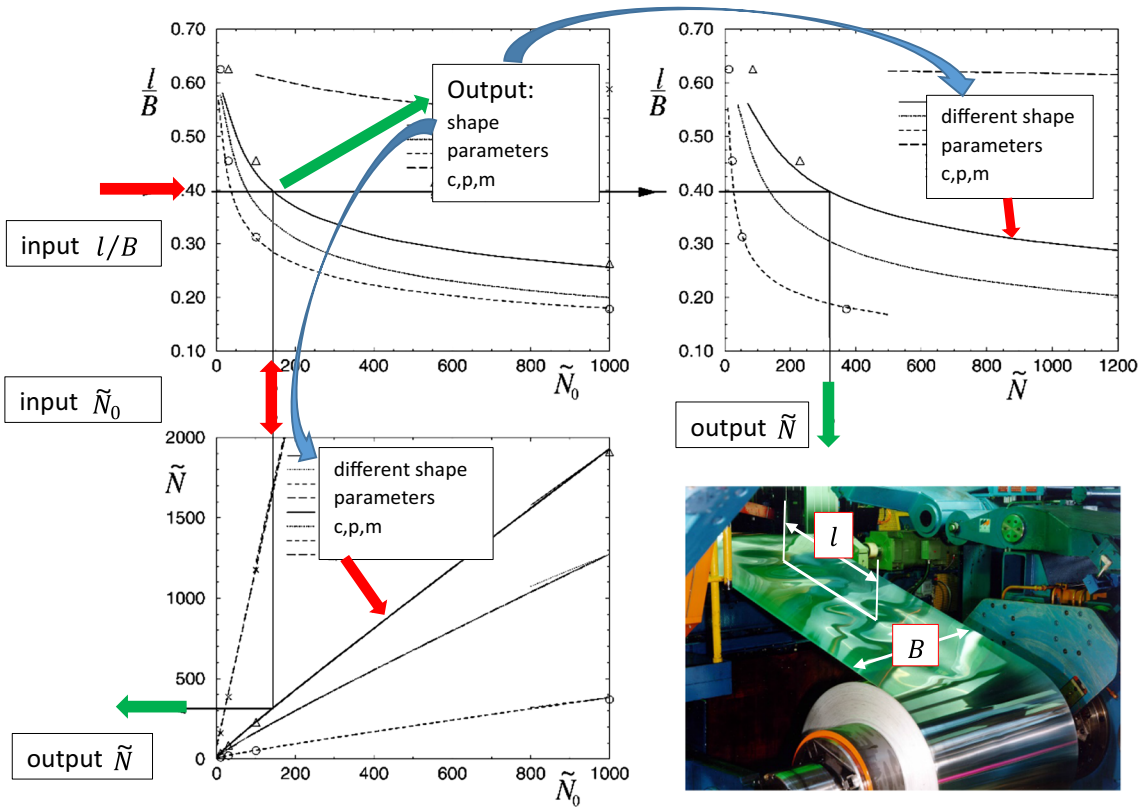

Fig. 17 Graphical representation of the solution strategy for solving the inverse problem (photograph by courtesy of Voestalpine, Linz)

enough to prevent the strip from showing wavy deformations (the β values correspond to those in Fig. 18), and moving along the path from right to left towards full release (i.e. $\beta = 1.0$).

At the instant at which in Fig. 16 the path crosses the $\tilde{N}(\tilde{N}_0)$ line, the instability happens. This situation represents the bifurcation point in the diagram in Fig. 18. During continued release of the strip tension the

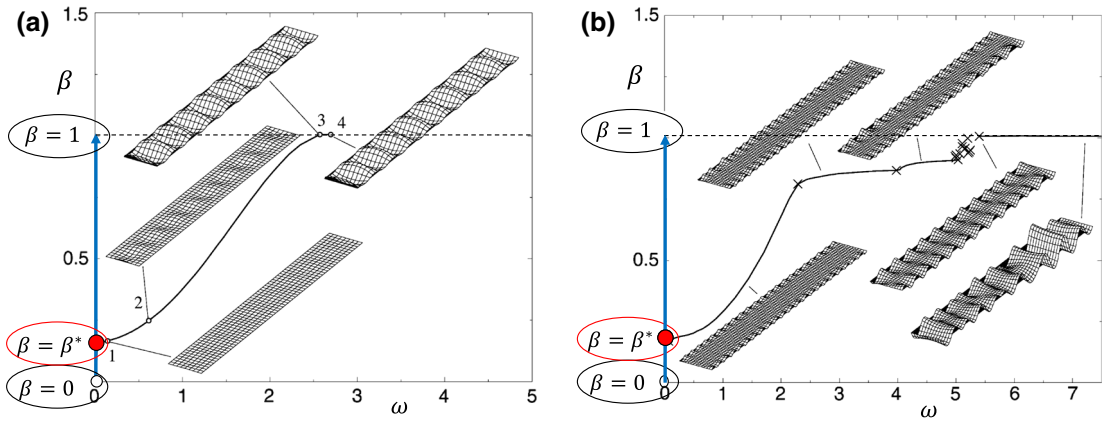

Fig. 18 Development of post-buckling deformations during release of the global strip tension; left: centre waves (see also Fig. 16); right: edge waves

amplitude of the waves increases, and under certain circumstances post-buckling bifurcations may appear, as shown in Fig. 18. Another kind of post-buckling process, in which the strip is laid down onto a plane surface during tension release (as done in practice for the sake of quality inspection) is simulated in [24].

The post-buckling bifurcations in Fig. 18b are the consequence of initial imperfections introduced as a random pattern in the simulation.

Here, the correctness of the statement according to which buckling under tensile load is caused by local compressive stresses is obvious and needs no further discussion.

5 Thin films

In materials sciences, some other, probably less known, but interesting examples of instabilities under global tensile load can be found. For instance, if a strip consisting of a thin metallic film (some nanometres thick) on a polymeric substrate (some micrometres thick) is stretched, the following observations can be made.

At a certain global tensile strain of the strip specimen, the metallic film starts cracking with so-called channel cracks running perpendicularly to the loading direction. With further stretching, the crack density grows up to eventual saturation [25].

Further stretching leads to local "film buckling", accompanied by delamination and progressive uplift of the film from the substrate; see Fig. 19.

Certainly, also in this buckling problem under global tensile loading local compressive stresses in the film are the reason for the instabilities. Where do these, let's call them "transverse compressive stresses", come from?

(i) One reason could be a mismatch in the Poisson's ratios between film and substrate, $\nu_\mathrm{f} \neq \nu_\mathrm{s}$ (subscript f stands for film and s stands for substrate).
Based on experimental observation and on computational results [25], it can be assumed that, due to the clamping boundary conditions, the stretched, but still uncracked specimen does not show any curvature in the area under consideration (i.e., in the middle of the specimen) during the experiment. Thus, as long as the film, the substrate, and the interface are intact, in-plane strain coupling exists between film and substrate in both longitudinal and transverse directions. This, in combination with the equilibrium condition (no resultant force in transverse direction), allows the estimation of the transverse film stress σ_f as a function of the global stretch ε_L of the specimen in longitudinal direction:

$$\sigma_\mathrm{f} = \frac{(\nu_\mathrm{f} - \nu_\mathrm{s})\, E_\mathrm{f}}{1 - \nu_\mathrm{f}^2 + \left(1 - \nu_\mathrm{s}^2\right) \frac{E_\mathrm{f} t_\mathrm{f}}{E_\mathrm{s} t_\mathrm{s}}} \varepsilon_\mathrm{L} \ . \tag{38}$$

In situations, in which $\nu_\mathrm{f} < \nu_\mathrm{s}$, transverse compression stresses develop, when stretching the specimen. However, much more important and nearly independent of any Poisson's mismatch is the following reason for transverse compressive stresses in the film.

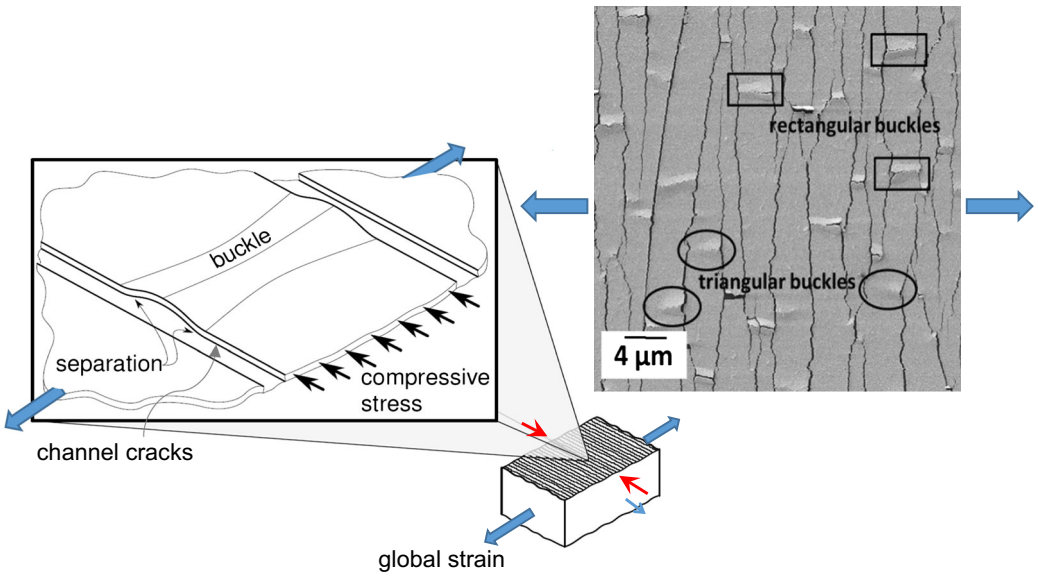

Fig. 19 Cracking and buckling of a thin metallic film on a polymeric substrate under global tensile loading (photograph—see [26]—by courtesy of ESI, Leoben)

(ii) Since in the experiments no local buckling is observed before saturation of the crack density is achieved, another model can be developed for explaining the appearance of transverse compressive film stresses and determining their intensity as function of the amount of stretch. The film cracking process leads to a continued stress redistribution in the system, and after saturation further stretching of the specimen will not lead to significant increase in the longitudinal stretch in the film substrips, each of them between two adjacent channel cracks, but simply enlarges the width of the channel cracks between them. Just for the sake of simplicity, let us assume that then the channel cracks are narrow enough so that the in-plane stresses in longitudinal direction of the specimen, L, are negligibly small. Under this (certainly rather roughly simplifying) assumption, the transverse compression stresses develop with further stretching the specimen as follows:

$$\sigma_{\mathrm{f}} = \frac{E_{\mathrm{f}}\nu_{\mathrm{f}}}{\frac{E_{\mathrm{f}}}{E_{\mathrm{s}}} + \left(1-\nu_{\mathrm{f}}^2\right)\frac{t_{\mathrm{f}}}{t_{\mathrm{s}}}}\varepsilon_{\mathrm{L}}. \tag{39}$$

Both Eqs. (38) and (39) overestimate the transverse compression stress. In (38), no cross-bending is taken into account, and in (39) very narrow substrips are assumed, i.e. the minimum crack distance, which is determined by shear leg considerations (see [25] is small enough to hinder the development of substantial membrane stresses in the global longitudinal orientation. Anyway, in the following considerations these simplifications are no longer used.

The experimental treatment and computational simulation of the above-mentioned cracking and stress redistribution processes are published in detail in [25]. Figure 20 shows some new results of extended simulations.

In [26], it is shown how from experimental considerations in combination with an analytical model or, more precisely, using computational models [13] interface strength parameters can be deduced, again in terms of solving an inverse problem. The knowledge of the interface strength parameters of such compounds, which due to the small geometrical conditions hardly can be measured directly, is crucial for the design and manufacture of electronic devices, particularly of flexible electronic devices.

In order to get the basis for determining the interface parameters the whole complex process of stretching → cracking → crack density saturation → local buckling with delamination at the buckles, has to be simulated. Due to the strong nonlinearities and, especially, because of the three-dimensional character of the process, analytical solutions (as were obtained in simplified two-dimensional models in [26]) are no longer sufficient, but nonlinear finite element modelling and analysis in combination with carefully performed experiments are the proper choice of methods. As results of a multi-scale analysis strategy, developed in [13,25], the global stretch, which leads to film buckling of a given film substrate specimen, can be calculated and compared

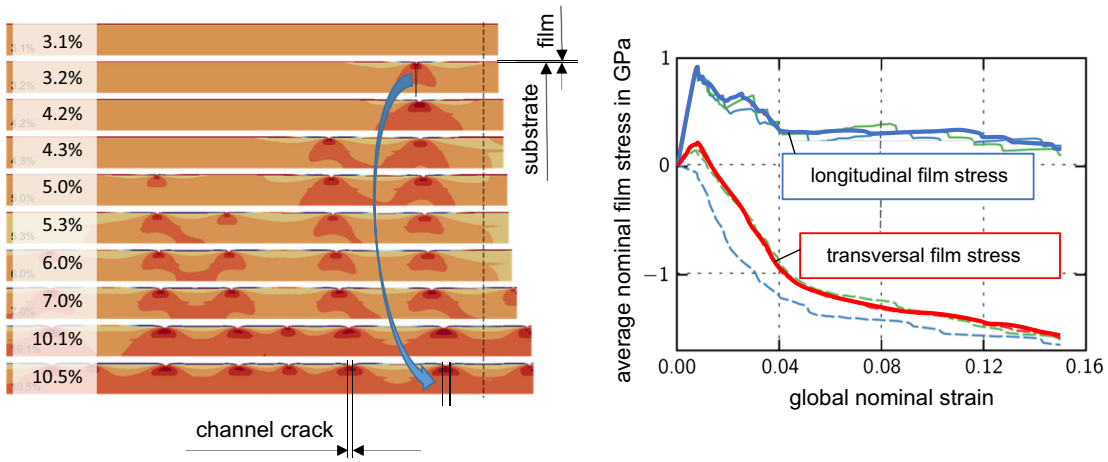

Fig. 20 Evolution of the crack pattern and volume-averaged in-plane stresses in the film, simulated as some sort of stochastic process [25]

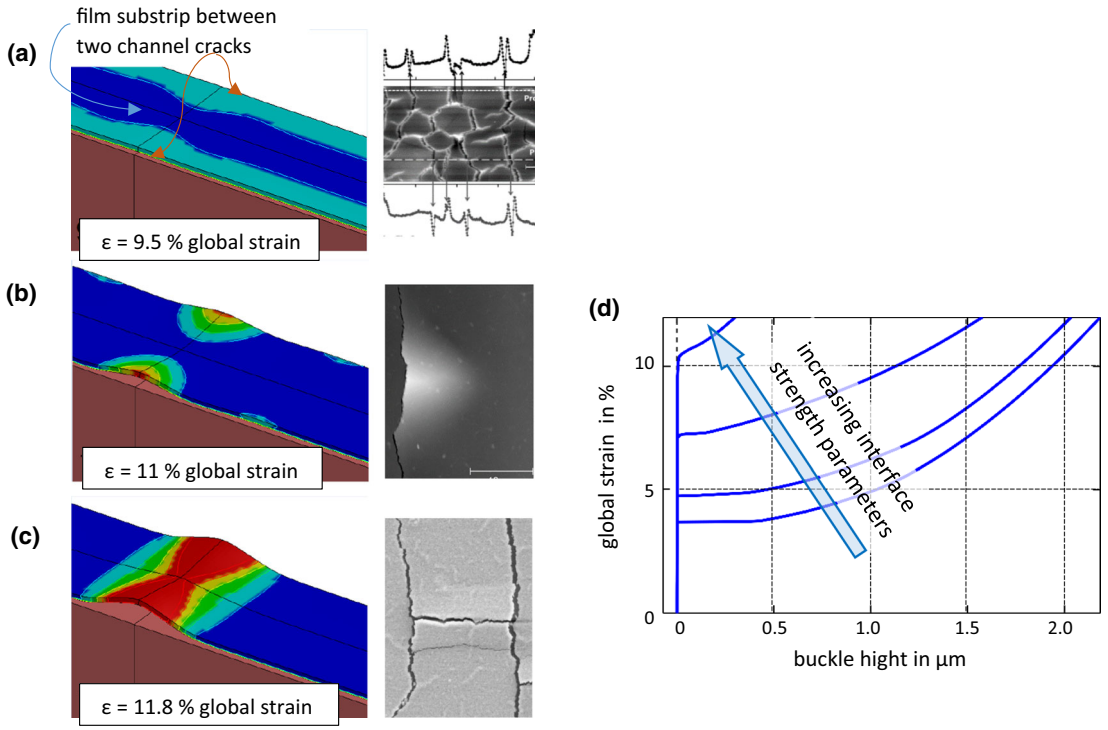

Fig. 21 Process: mode II debonding (**a**) → buckling and mode I debonding → post-buckling (**b**, **c**); bifurcation diagram (**d**); compare [13]

with the stretch value, at which in the experiment the instant of buckling is observed. Variation in the so long unknown interface strength parameters, which are input to the cohesive zone elements in the simulation model, until coincidence between calculated and measured critical stretch is achieved, leads to an estimate of the real interface strength. This means that for the cohesive zone model used in [13], the maximum normal debonding stress during uplift, $\hat{\sigma}$, at which interface damage starts, and the Griffith' energy release rates for mode I , G_{I}^{c}, and for mode II, G_{II}^{c}, respectively, have to be varied appropriately. For more advanced cohesive zone models for simulating debonding of the film from the substrate, see [27].

Figure 21 shows, from simulation and experimental results, what happens if the global stretch approaches the critical value and surpasses it. In Fig. 21a, the edges of the substrips curve upwards and interface failure according to fracture mode II is initiated. In Fig. 21b, it is shown how the increase in the specimen's stretch leads

to localization of this interface failure and film uplift starts by forming triangular buckles. The interface failure changes now from mode II to mode I; triangular buckles expand and develop to become rectangular buckles accompanied by rapid delamination growth with increased specimen stretch; see Fig. 21c. The calculated stretch–uplift diagram as shown in Fig. 21d demonstrates the character of the process as bifurcation buckling.

6 Conclusions

Buckling is a possible mode of failure of thin walled or slender structures not only under compression, but also under tensile loading. Nevertheless, it should be mentioned that, even if the external load is tensile, the stress state, which leads to instability, is always compressive. Thus, one should be clear in wording and talk about "buckling under tensile loads" instead of simply saying "buckling under tension". Buckling phenomena under tensile loading have been demonstrated for beams with rigidly connected rods at the ends (starting with "Ziegler's beam"), on stretched plates with and without holes or cracks, on rolled metal strip with residual stresses caused by the rolling process, and on thin metallic films bonded to polymeric substrates. While buckling in most cases is an unwanted phenomenon, in the latter example buckling and post-buckling investigations are used for determining interface strength parameters which hardly can be measured directly.

Acknowledgements Open access funding provided by TU Wien (TUW). Parts of the paper stem from a project financially supported by the Austrian Science Funds (FWF) under the project number P 22648. Furthermore, the contributions from colleagues from the TU Wien, the Montanunversität (MU) Leoben, from the Erich Schmid Institute (ESI) of the Austrian Academy of Sciences, from the Max-Planck-Institut für Eisenforschung GmbH (Düsseldorf), as well as from the industrial partners (BWG Duisburg) to the papers are acknowledged. Their names are in the authors lists of the respective papers.

Appendix

In Sect. 2, a virtual system of an elastically pinned rod with two degrees of freedom is mentioned. It is described in Fig. 22. The post-buckling behaviour of the real system (Ziegler's beam) shows that the moveable support for a while moves towards the other support and at a certain load intensity turns back to the initial position. At the same time, the deflection increases initially and at the same certain load intensity it starts decreasing. It is shown now that the virtual system described here qualitatively represents the behaviour of the real system, what quite obviously a rod, just pinned at one end cannot do.
From the equilibrium conditions of the nontrivial configuration with $0 < \varphi \ll 1$:

$$F - S = 0, \quad Fe\varphi - Sf\varphi - \gamma\varphi = 0 \tag{40}$$

(S is the tensile force in the spring), one gets the critical load

$$F_{\text{crit}} = \gamma / (e - f)\,. \tag{41}$$

With respect to the critical load F_{crit}, the second degree of freedom, i.e. the mobility of the support, does not play any role. Hence, the existence of a second degree of freedom does not perturb the argument stated in

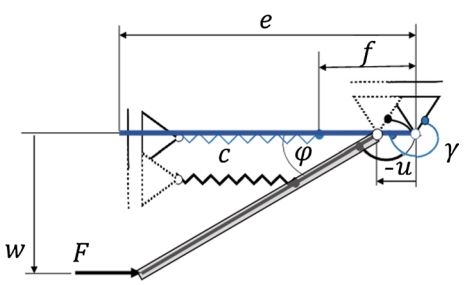

Fig. 22 Virtual system for Ziegler's beam

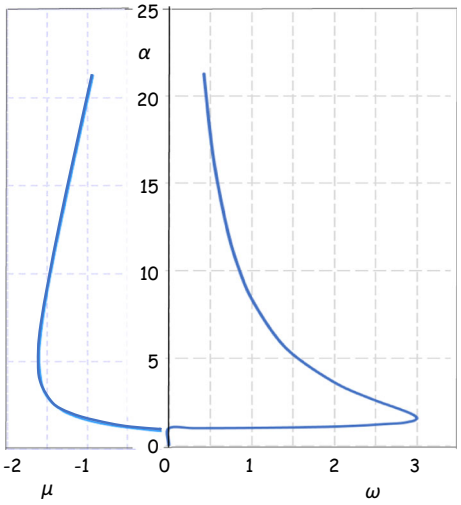

Fig. 23 Post-critical behaviour of the virtual two-degree-of-freedom system

Sect. 2, according to which the simple virtual pinned rod system with one degree of freedom underpins the fact, that it is not the beam which buckles, but the rod.
However, in order to provide a simple virtual system for the post-buckling behaviour of Ziegler's beam, the second degree of freedom is essential.
Let us introduce the following dimensionless quantities:

$$\kappa = e/f - 1,\ \alpha = F\,(e - f)\,/\gamma,\ \mu = u/f,\ \omega = w/f,\ \text{and}\ \phi = \gamma/(ce^2). \tag{42}$$

With these notations, the dimensionless critical load gets $\alpha_{\text{crit}} = 1$, and equilibrium in the post-buckling regime, i.e. $\alpha > 1$ and $0 < \varphi \leq \pi$, leads to the following equations for the description of the post-buckling configuration:
For given values of κ and ϕ and the rotation angle φ as function of the load intensity α, determined by

$$\alpha \sin\varphi - \varphi = 0 \tag{43}$$

the post-critical movement of the system with monotonically increased load ($\alpha > 1.0$) is given by

$$\mu\,(\alpha) = \frac{\alpha\phi}{\kappa} - 1 + \cos\varphi\,(\alpha)\,, \qquad \omega\,(\alpha) = (1 + \kappa)\sin\varphi\,(\alpha)\,. \tag{44}$$

These results are shown in Fig. 23 for $\kappa = 2.0$ and $\phi = 0.1$.
Even so, for the sake of simplicity, the springs are modelled as linear elastic, the comparison between Figs. 4 and 23 shows that the principal characteristics of the post-buckling behaviour are captured by the virtual system.

References

1. Ziegler, F.: Mechanics of Solids and Fluids, 2nd edn. Springer, Berlin (1995)
2. Ziegler, H.: Principles of Structural Satbility, 1st edn. Blaisdell Publishing Company, New York (1968)
3. Ziegler, F., Rammerstorfer, F.G.: Thermoelastic stability. In: Hetnarski, R.B. (ed.) Thermal Stresses III, pp. 107–189. North-Holland Publishing Company, Amsterdam (1989)
4. Daxner, T., Rammerstorfer, F.G., Fischer, F.D.: Instability phenomena during the conical expansion of circular cylindrical shells. Comput. Methods Appl. Mech. Eng. **194**, 2591–2603 (2005)
5. Datta, P.K., Biswas, S.: Research advances on tension buckling behaviour of aerospace structures: a review. Int. J. Aeronaut. Space Sci. **12**, 1–15 (2011)
6. Brighenti, R.: Buckling sensitivity analysis of cracked thin plates under membrane tension or compression loading. Nucl. Eng. Des. **239**, 965–980 (2009)
7. Tomita, Y., Shindo, A.: Onset and growth of wrinkles in thin square plates subjected to diagonal tension. Int. J. Mech. Sci. **30**, 921–931 (1988)
8. Segedin, R.H., Collins, I.F., Segedin, C.M.: The elastic wrinkling of rectangular sheets. Int. J. Mech. Sci. **30**, 719–732 (1988)

9. Friedl, N., Rammerstorfer, F.G., Fischer, F.D.: Buckling of stretched strips. Comp. Struct. **78**, 185–190 (2000)
10. Rammerstorfer, F.G., Pahr, D.H., Daxner, T., Vonach, W.K.: Buckling in thin walled micro and meso structures of lightweight materials and material compounds. Comput. Mech. **37**, 470–478 (2006)
11. Daxner, T., Pahr, D.H., Rammerstorfer, F.G.: Micro- and meso-instabilities in structured materials and sandwich structures. In: Falzon, G., Aliabadi, M.H. (eds.) Buckling and Postbuckling Structures: Experimental, Analytical and Numerical Studies, pp. 453–495. Imperial College Press, London (2008)
12. Rammerstorfer, F.G., Fischer, F.D., Friedl, N.: Buckling of free infinite strips under residual stresses and global tension. J. Appl. Mech. **68**, 399–404 (2001)
13. Toth, F., Rammerstorfer, F.G., Cordill, M.J., Fischer, F.D.: Detailed modelling of delamination buckling of thin films under global tension. Acta Mater. **61**, 2425–2433 (2013)
14. Buckingham, E.: On physically similar systems; illustrations of the use of dimensional equations. Phys. Rev. **4**, 345–376 (1914)
15. Shimizu, S.: Tension buckling of plate having a hole. Thin Walled Struct. **45**, 827–833 (2007)
16. Bringhenti, R.: Buckling of cracked thin plates under tension or compression. Thin Walled Struct. **42**, 209–224 (2005)
17. Jacques, N., Portier-Ferry, M.: On mode localisation in tensile plate buckling. C. R. Mec. **333**, 804–809 (2005)
18. Sipos, A.A., Fehér, E.: Disappearance of stretch-induced wrinkles of thin sheets: a study of orthotropic films. Int. J. Sol. Struct. **97–98**, 275–283 (2016)
19. Nayyar, V., Ravi-Chandar, K., Huang, R.: Stretch-induced wrinkling of polyethylene thin sheets: experiments and modeling. Int. J. Solids Struct. **51**, 1847–1858 (2014)
20. Rammerstorfer, F.G., Daxner, T.: Berechnungs- und Design-Konzepte für den Leichtbau. In: Degischer, H.P., Lüftl, S. (eds.) Leichtbau, pp. 14–49. Wiley-VCH, Weinheim (2009)
21. Firmberger, G., Rammerstorfer, F.G.: FEM simulations of buckling and post-buckling of stretched rectangular plates with cut-outs or cracks. ILSB-Report 299, TU Vienna (2017)
22. Abdelkhalek, S., Zahrouni, H., Legrand, N., Potier-Ferry, M.: Post-buckling modelling for strips under tension and residual stresses using asymptotic numerical method. Int. J. Mech. Sci. **104**, 126–137 (2015)
23. Fischer, F.D., Rammerstorfer, F.G., Friedl, N.: Residual stress-induced center wave buckling of rolled strip metal. J. Appl. Mech. **70**, 84–90 (2003)
24. Fischer, F.D., Friedl, N., Noé, A., Rammerstorfer, F.G.: A study of the buckling behaviour of strips and plates with residual stresses. Steel Res. Int. **76**, 327–335 (2005)
25. Marx, V.M., Toth, F., Wiesinger, A., Berger, J., Kirchlechner, C., Cordill, M.J., Fischer, F.D., Rammerstorfer, F.G., Dehm, G.: The influence of a brittle Cr interlayer on the deformation behavior of thin Cu films on flexible substrates: experiment and model. Acta Mater. **89**, 278–289 (2015)
26. Cordill, M.J., Fischer, F.D., Rammerstorfer, F.G., Dehm, G.: Adhesion energies of Cr thin films on polyimide determined from buckling: experiment and model. Acta Mater. **58**, 5520–5531 (2010)
27. Mukherjee, B., Barta, R.C., Dillard, D.A.: Edge debonding in peeling of a thin flexible plate from an elastomer layer: a cohesive zone model analysis. J. Appl. Mech. (2017). https://doi.org/10.11115/1.4034988